FERMILAB-PUB-13-321-AD

Evidence for OTR Linear Polarization Effects in Beam-Profile Monitors*

A.H. Lumpkin, A.S. Johnson, J. Ruan, R. Thurman-Keup, Fermilab, Batavia, IL U.S.A. 60510
C.-Y. Yao, Argonne National Laboratory, Argonne, IL U.S.A. 60439
P. Evtushenko, Thomas Jefferson National Laboratory, Newport News, VA 23606

Abstract

Investigations of the effects of optical transition radiation (OTR) polarization components on beam profiles are presented. The transverse profiles are examined using the OTR perpendicular and parallel polarization components with respect to the dimension of interest. We observed ~15% projected profile size reductions with the perpendicularly polarized components on a 65-µm beam image size case at 14 MeV, a 150-µm beam image size at 4.5 GeV, and a 1200-µm beam image size at 7 GeV. These effects are all several times larger than expected from the standard OTR point-spread function calculations. We propose the time-averaged induced current distribution which generates the OTR represents the actual beam size more faithfully with the perpendicular polarization component and recommend its routine use and subsequent deconvolution.

Key words: OTR, linear polarization, beam size

Index: 41.60.Cr

*Work supported by U.S. Department of Energy, Office of Science, Office of High Energy Physics, under Contract No. DE-AC02-06CH11357.

I. INTRODUCTION

The characterization of the transverse beam size of relativistic electron beams using optical transition radiation (OTR) imaging [1-3] has been implemented at many accelerators in the last two decades. OTR imaging had been considered a reliable method for obtaining beam profiles [4-7] prior to the identification of the microbunching instability and its concomitant coherent intensity fluctuations that are evident in many compressed bright beams [8-12]. Besides that issue, theoretical modeling has identified only minor polarization effects in the point-spread function (PSF) [5] or single-particle function [6]. However, we examine empirical evidence [13-17] that the utilization of the polarization component orthogonal to the dimension of interest results in a noticeably smaller observed projected image profile than theoretically predicted [4-6]. In those calculations the OTR point spread function width was in the few-micron range for 0.10 rad collection angles so only experiments that involve beam sizes with sigma <20 microns might be concerned. In practice most beam-profiling experiments have not considered the OTR polarization effects, investigators did not install linear polarizers in their optical transport lines, and their effective collection angle was reduced by a final lens stop. A previously unpublished OTR result at 7 GeV on a transport line exhibited apparent polarization effects at the 1200-µm regime although only the optical diffraction radiation (ODR) polarization results were explicitly reported [15]. These OTR data are now reported, as well as a similar effect within the OTR/ODR tests at Jefferson National Lab (JLAB) at 4.5 GeV in the 125- to 300-µm regime [16].

We have recently continued investigations of this phenomenon at low gamma at Fermilab with a more controlled experiment where the linear polarizers are selectable in a filter wheel which also included a clear glass position to compensate for the optical path. The aperture for light collection at the polarizer position is thus kept fixed compared to the previous tests at FNAL and JLAB [13, 16]. At the relatively low gamma of ~30, the horizontal polarization component of OTR is more asymmetric than the vertical one in our optical solid angle. We still observed 11-18% projected profile size

reductions on a 65-µm beam size case with the perpendicularly polarized components. This similar anomalous effect of ~15% (which was observed over two orders of magnitude in gamma and a factor of 20 in beam size in these collected experiments) is compared to results from a standard OTR point-spread-function (PSF) model [4-6]. The potential for overestimating beam sizes with OTR imaging is addressed in this paper.

II. EXPERIMENTAL ASPECTS

The most recent tests were performed at the Fermilab A0 photoinjector (A0PI) facility which includes an L-band photocathode (PC) rf gun and a 9-cell SCRF accelerating structure which combine to generate up to 16-MeV electron beams. The drive laser operates at 81.25 MHz although the micropulse structure is divided down to 1 MHz rate. Due to the low electron-beam energies and low OTR signals, we typically summed over micropulses depending on the charge per micopulse. Micropulse charges from 25 to 500 pC were used for beam sigma sizes of 45 to 250 microns. Initial experiments were performed at station X5 comparing OTR with a powder scintillator [17,18]. Subsequently, the prototype station was installed in the user beam line section beyond the horizontal spectrometer in the straight ahead line as indicated in Fig. 1. The nominal beam parameters are given in Table 1. We integrated signal over 10-50 micropulses to obtain adequate OTR signal.

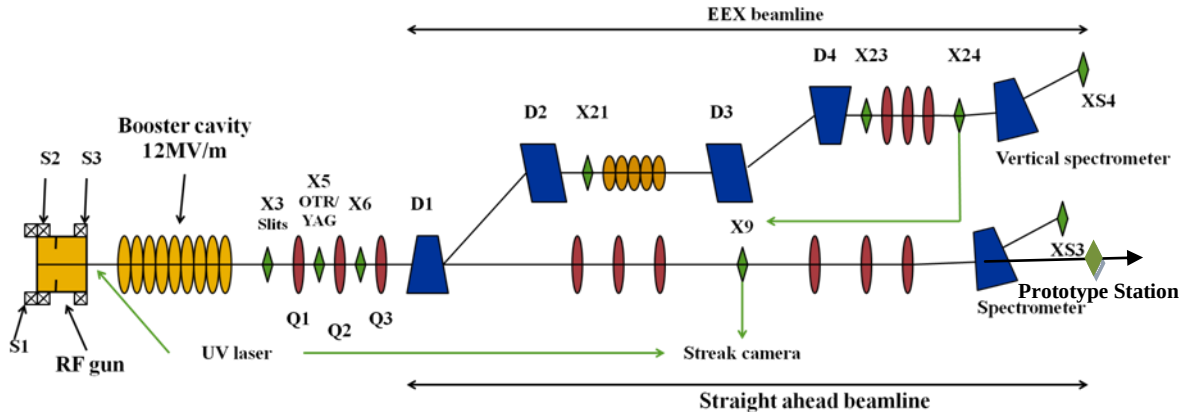

Figure 1: A schematic of the A0 photoinjector test area showing the PC rf gun, 9-cell booster cavity, transverse emittance stations, the OTR stations, the streak camera, and the EEX beamline. The X5 and prototype station locations are indicated.

Table 1: Summary of nominal electron beam parameters for operations at A0PI with 250 pC per micropulse and a drive laser bunch length of 2.7 ps (sigma).

Parameter	**Units**	**Value**
Energy	MeV	15
Energy spread	kev	10-15
Transverse Emittance	mm mrad	2.6 ± 0.3
Bunch length (σ)	ps	3.1 ± 0.3

The prototype station (see Fig. 2) consists of a vacuum cross with a three-position pneumatic actuator allowing selection of a beam-impedance matching screen, a 100-μm thick YAG:Ce single crystal with its surface normal to the beam direction followed by a 45 degree turning mirror, or a 1-μm thick Al foil for OTR followed by a 45 degree turning mirror. For the OTR polarization tests we removed the thin first foil and used the turning mirror as the OTR screen. We refocused the optics by translating the optical assembly back from the viewing window by 12.5 mm so the center of this OTR screen was in focus. For these tests both turning mirrors were an aluminized Si substrate (200 μm thick). As part of the optics design, a back-illuminated virtual target option with matched field lens could be selected by inserting a beam splitter into the relay optics path. This scene was then relayed to the final Computar zoom lens mounted on the 1.3 Megapixel Prosilica CCD camera and used for resolution and optics calibration aspects. The optical resolution tests were reported previously [8]. A filter wheel was used to select neutral density filters or one of the two linear polarizers which were oriented with the axes in the horizontal and vertical directions. This prototype station was constructed by RadiaBeam Technologies under a contract with Fermilab.

The optical system has 14 (7) μm rms spatial resolution when covering a vertical field of view (FOV) of 18 (5) mm. The calibration factors were 18.2 μm per pixel and 5.3 μm per pixel, respectively. Because of the size of the polarization effects, the data are reported for the higher magnification and 5-mm FOV.

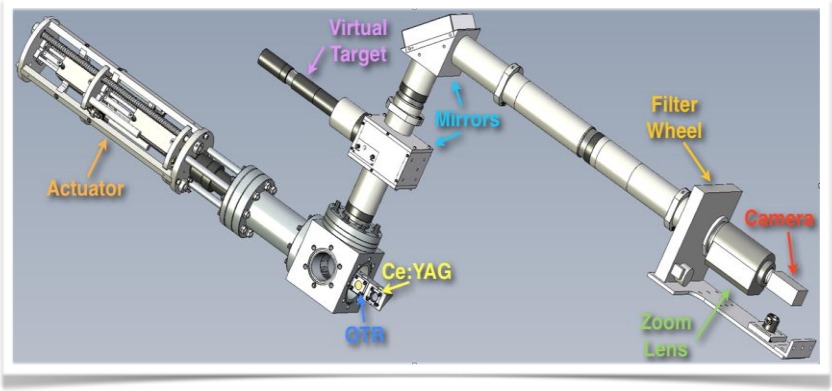

Figure 2: The prototype station with cube and actuator, screens, virtual target, optics, filter wheels, zoom lens, and camera.

The tests at JLAB were performed in one extraction line to a nuclear physics test area in Hall-A and were motivated by an interest in optical diffraction radiation (ODR) as a nonintercepting beam size monitor for the operational beam line. The details are provided in reference [16]. The electron beam energy was 4.5 GeV with beam sizes of about 125 to 300 µm depending on the upstream focusing quadrupoles' settings. A wire harp was located in close z proximity to the OTR/ODR station and served as an independent beam-size monitor for low-power beam. The camera was a JAI-A60 CCD with a National Instruments 10-bit frame grabber/digitizer. A key point is the linear polarizers were on a holder on a flipper actuator so they provided a 25-mm diam aperture when inserted and no aperture when withdrawn. The calibration factors were about 10.9 µm/pixel in x and y directions.

The tests at the Advanced Photon Source (APS) were performed in the Booster ring extraction (BTX) line which provided 7-GeV single micropulses containing up to 3.2 nC each at 2 Hz. The details of the OTR/ODR station are provided elsewhere [15] and predated the tests at JLAB and Fermilab. The optics included a field lens and relay optics with filter wheels providing the options for the linear polarizers or neutral density filters. These were the first reported near-field focusing tests with ODR, and we referenced our images to the observed OTR beam image sizes at the same screen location when the screen was inserted fully and intercepted the beam. Due to the larger beam sizes and field of view used at APS, calibration factors of 60 µm and 46 µm per pixel for x and y axes, respectively, were

employed at 7 GeV. In the course of the ODR tests, we observed significant polarization impacts on the images as predicted by the analytical model [15]. The online image processing indicated polarization effects in the OTR as well, but we have now recently also post-processed those same images individually using a different Gaussian fitting routine to evaluate statistical errors more carefully.

III. OTR POINT-SPREAD-FUNCTION MODEL

The fundamental OTR mechanism occurs when a charged particle beam transits the interface between two media [1]. The approaching charge and the induced image charge in the second medium may be treated as a collapsing dipole with the consequent emission of radiation, i.e. OTR. The yield is about 1 visible photon per 1000 electrons incident, but they are emitted in the few-fs time scale as compared to the slower 80-ns scintillation process. The radiation is emitted around the angle of specular reflection for backward radiation and around the angle of the beam direction in the forward direction for high gamma beams. For an oblique incidence such as 45 degrees, backward OTR is emitted at 90 degrees to the beam direction. This geometry is compatible with most accelerator beam profiling stations.

The assessment of the actual OTR PSF has to first order been described by several authors previously [4-7]. The model invokes the convolution of the basic OTR single particle angular distribution function with the J_1 ordinary Bessel function to describe the intensity pattern at the detector. The concept is to calculate the electric field distribution at the image plane and then square it to get the photon intensity distribution I(x, y) expected. This is described in ref. [8,9] and shown in the expression below for a single ideal lens:

$$I(x,y) \propto \left[\int \frac{\theta^2}{\theta^2 + 1/\gamma^2} \cdot J_1\left(\frac{k\theta\sqrt{x^2+y^2}}{M} \right) d\theta \right]^2,$$

where $k = 2\pi/\lambda$ with λ the wavelength of radiation , x and y are the spatial coordinates, M is the magnification, the angle of OTR emission is θ, and the Lorentz factor is γ. The angle of integration is limited by the aperture of the lens (θ_{max}), and this can have a strong effect on the PSF in the model.

Because at the simplest level OTR is inherently radially polarized, the point spread function does reflect this aspect in the upper left image of Fig. 3. Note the axes scales are ±100 μm. The horizontal polarization component appears as a double lobe as seen in Fig. 3b, while the vertical polarization is seen also as a double lobe in Fig. 3c. These are *not* far-field angular distribution patterns, but the PSF in the image plane. The projections of these are shown overlaid in Fig. 4a where the total (blue curve), horizontal polarization with horizontal projection (red curve), and horizontal polarization with vertical projection (green curve) exhibit different features.

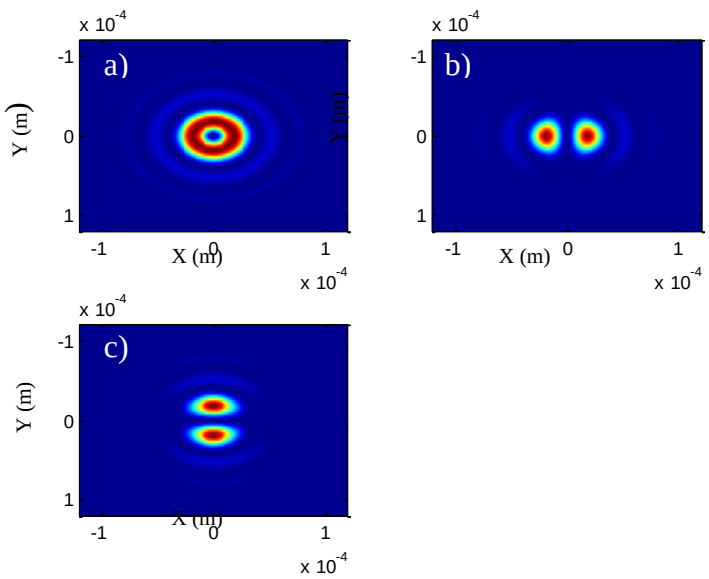

Figure 3: OTR PSF images with a) total, b) horizontal polarization, and c) the vertical polarization of the case: Energy=14.3 MeV, M=1, λ=500 nm, and θ_{max}=0.010. The two axes scales are different and cause the elliptical aspect in the images.

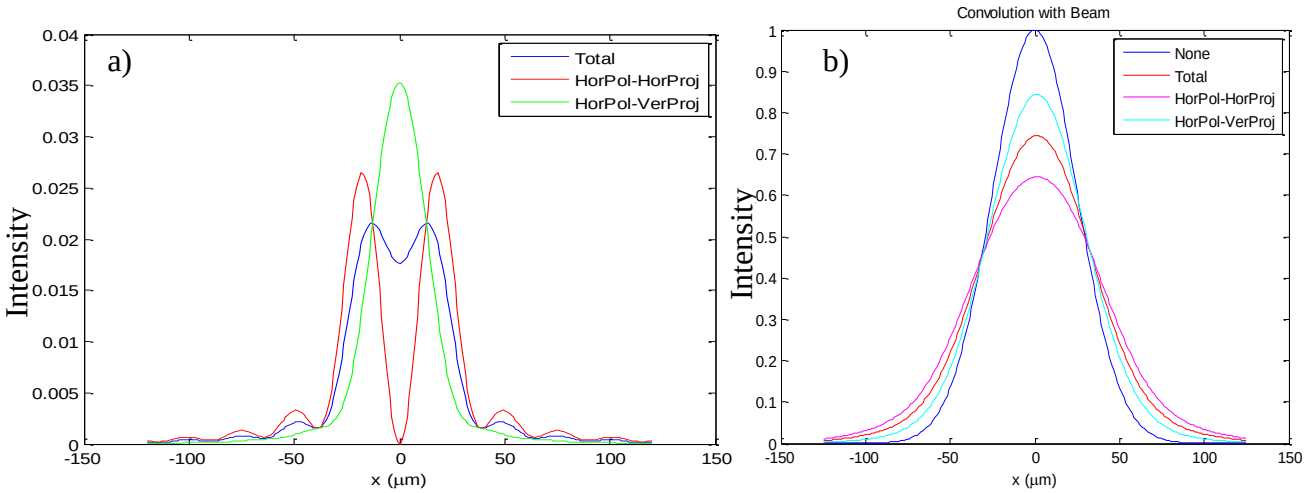

Figure 4: a) OTR PSF projections of the images in Fig. 3 with total, horizontal polarization with horizontal projection, and the vertical projection of the same case. b) Comparison plots of the original x size (25 μm) with no convolution and convolutions with the OTR PSF projections of the total (33.1 μm), horizontal polarization-horizontal projection (38.0 μm), and the vertical projection (29.3 μm) of the same latter case.

We next show in Fig. 4b the results of convolving the initial beam size of σ=25 μm with the OTR PSF projections of Fig. 4a: The results of the Gaussian fits to the convolved profiles are: total=33.1 μm, horizontal polarization=38.0 μm, and the vertical projection of the horizontal polarization=29.3 μm. The model does support the concept that use of the perpendicularly polarized component is closer to the original 25 μm size than using the total or parallel components. Even in this vertical projection case one would still need to deconvolve the PSF to get the actual beam size. This several-micron effect was generated by using the 10-mrad acceptance angle, which is smaller than one might expect for our optics and a two times smaller beam size. The results in Fig. 5 for convolving an initial 50-μm beam size and the OTR PSF using the same optical parameters as in Fig. 3 are: total=55.6 μm, horizontal polarization=58.5 μm, and vertical projection=53.0 μm. The effects are relatively smaller and symmetrically change around the total value. In this case the 2.6-μm reduction in the convolved total OTR profile sigma versus the perpendicular one is indicated, and both are larger than the initial beam size. For a 100-μm initial beam size for the same parameters, the effect is even smaller and even more difficult to detect in practice.

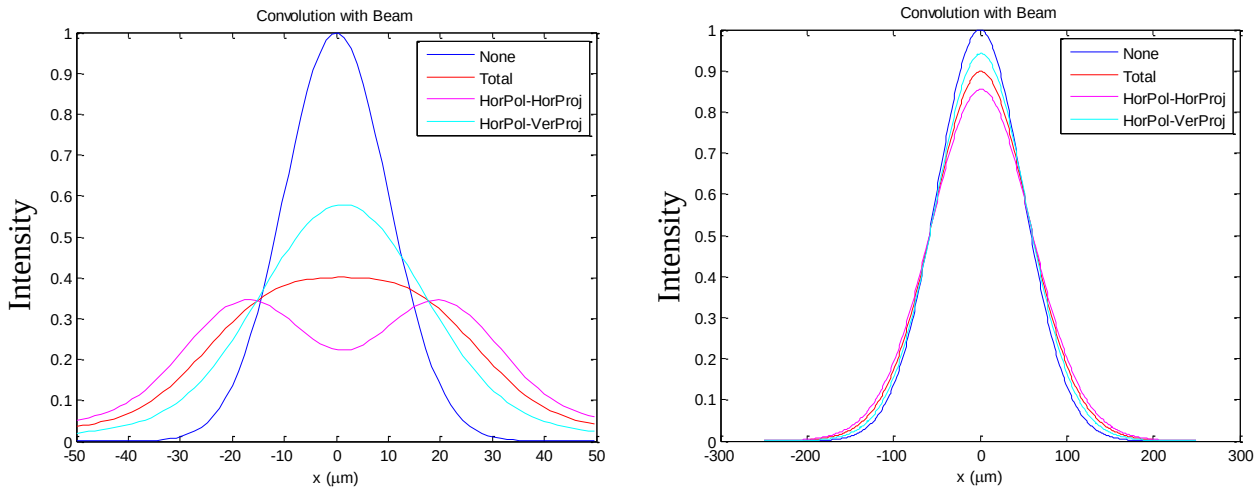

Figure 5: Comparison plots of the original x size 10 μm (left) and 50 μm (right) with no convolution and convolutions. The 50-μm case was convolved with the OTR PSF projections of the total (55.6 μm), horizontal polarization-horizontal projection (58.5 μm), and the vertical projection (53.0 μm) of the same latter case.

A more extreme case is described in reference [19] where the beam size in the vertical plane is only 2.2 μm, and the polarized PSF's double lobe for their optical system with magnification of 18 is actually visualized in the image such as indicated in the 10-μm case shown in Fig. 5(left). Those authors used the visibility of the valley between the lobes to deduce the small beam sizes.

IV. EXPERIMENTAL RESULTS

14.3-MeV Case (Fermilab)

The fundamental issue is whether one can detect a measurable difference in beam profile sizes if one uses the perpendicular component of OTR, and if so, what is the magnitude? We used focusing by upstream quadrupoles to generate narrow vertical and horizontal stripes at the prototype station. Examples of the images are shown in Fig. 6. The total OTR is at the left and the vertically polarized at the right. The Gaussian fits are used on the projected profiles from the region of interest and are shown below each image. In this case they are 12.6±0.06 and 10.4±0.20 pixels, respectively. The results are tabulated in Table 2. The camera gain was adjusted to balance the signal levels being processed. Ten image individual averages were done with a MATLAB-based

image processing program, and the average variance was divided by $10^{1/2}$. We see an ~12-µm reduction (18%) in the initial 67-µm x size when using the perpendicular OTR component as compared to the two independent data sets taken with no polarizer.

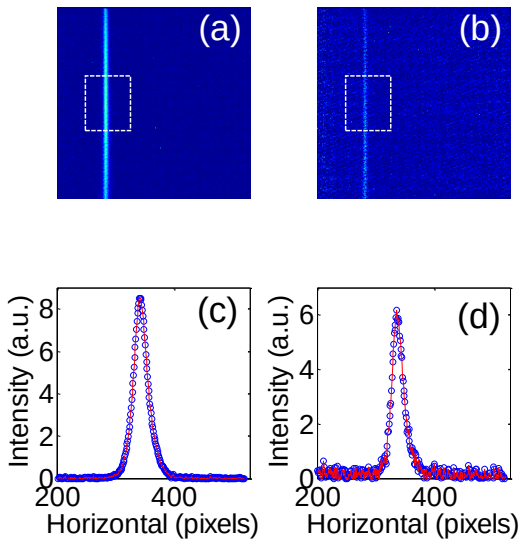

Figure 6: OTR images of vertical stripes a) total OTR and b) vertically polarized OTR. The projected x profiles from the region of interest are shown below each image.

Table 2: Summary of vertical-stripe data. The vertical (V) polarization data are indicated in determining the x sizes with the statistical uncertainty. The calibration factor was 5.3 µm per pixel.

Polarization	**X-sigma (pixel)**	**X-sigma (µm)**
No	12.6±0.06	66.8±0.3
V	10.4±0.20	55.1±1.1
No	12.7±0.07	67.3±0.4

Examples of the horizontal images are shown in Fig. 7. The total OTR is at the left and the horizontally polarized OTR image at the right. The Gaussian fits are used on the projected y profiles from the region of interest and are shown below each image. In this case they are 11.8±0.11 and 10.5±0.12 pixels, for y sizes of total and vertically polarized, respectively.

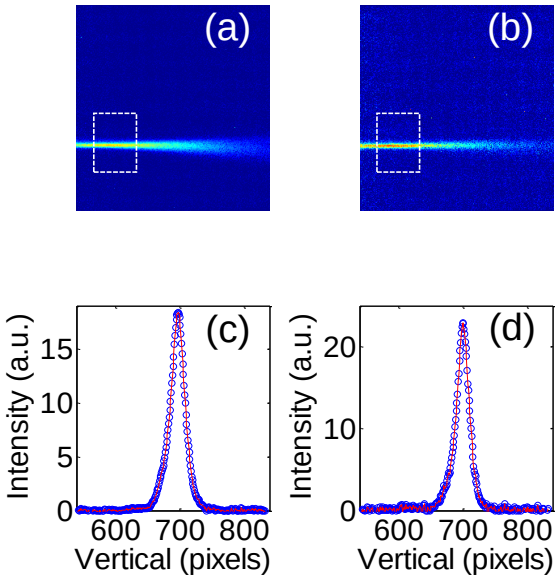

Figure 7: OTR images of horizontal stripes a) total OTR and b) vertically polarized OTR. The projected y profiles from the region of interest are shown below each image, c) and d) respectively.

The vertical size results are tabulated in Table 3. The digital camera's gain was adjusted to balance the signal levels being processed, and the same image processing was done. We see an ~7-µm reduction (11%) in the initial 62-µm y size with the perpendicular OTR component. This is based on averaging the three sets of data for each polarization state including a sequence change which are provided in Table 3 for completeness. We note that at this low gamma of ~30 with the screen rotation around a vertical axis, the horizontal polarized angular pattern is asymmetric in lobe intensity and shape while the vertical component lobes are symmetric. The broken symmetry in one plane is not in the model described in the next section, but is consistent with the smaller effect in the horizontal polarized component compared to Table 2.

Table 3: Summary of horizontal-stripe data. The horizontal (H) polarization data are indicated in determining the y sizes. The calibration factor is 5.3 µm per pixel.

Polarization	**Y-sigma (pixel)**	**Y-sigma (µm)**
No	11.8±0.11	62.5±0.6
H	10.5±0.10	55.7±0.6
No	11.5±0.10	61.0±0.6
H	10.5±0.10	55.7±0.6
H	10.2±0.09	54.1±0.5
No	11.6±0.12	61.5±0.6

4.5-GeV CASE (CEBAF/JLAB)

The results at CEBAF on OTR polarization effects have been reported previously within the ODR paper [16], but we include one figure for completeness here since there was a reference to the harp monitor data and have reprocessed the images for variance evaluations. These image sizes are an order of magnitude smaller than the 7-GeV cases of the next subsection in the major axis of the elliptical beam and at a similar gamma. The actual shape of the images changed from basically round (149 µm, 157 µm) with no linear polarizer to elliptical with the major axis parallel to the linear polarization axis selected and with the perpendicular minor axis being the dimension of interest. It is evident in Fig. 8 that the perpendicularly polarized component results are ~15% smaller than the total OTR x results and lie closer to the wire scan results over the range of x beam sizes from 380 to 160 µm. The error bars indicate the standard deviation of the mean value on the ten samples which included the machine's beam size fluctuations during data acquisition. This observed image size reduction is consistent with the hypothesis on the inherent advantage of the perpendicular polarization component of OTR.

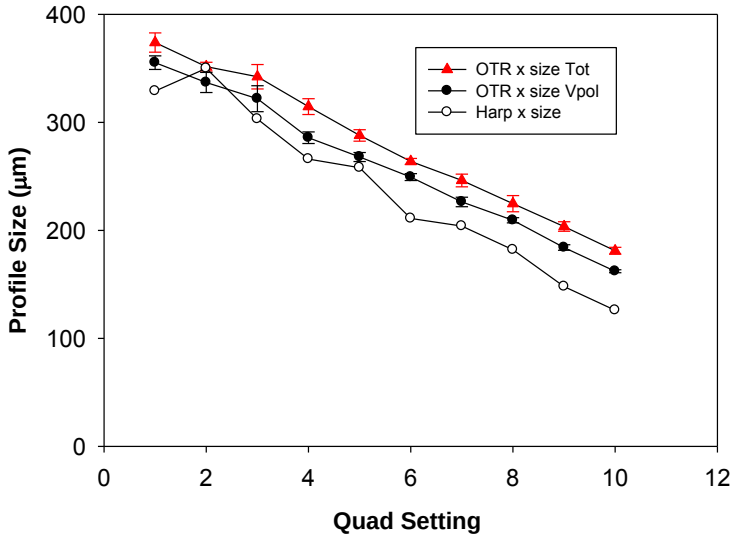

Figure 8: Comparison of the total OTR projected profiles in x, vertically polarized (Vpol) OTR results, and the wire harp results as a function of upstream quadrupole (Quad) settings at 4.5 GeV [16].

In addition, the more symmetric beam sizes in the 4.5-GeV data permitted comparison of the beam's y image size for the three OTR polarization cases as shown in Fig. 9. In this case, the parallel component (Vpol) is systematically larger than the total OTR projected case values, and the perpendicular case (Hpol) has the smaller values. This is qualitatively like the PSF model in Section 3 results, except the magnitude of the differences are much larger than 2-3 µm, and the beam size is almost 2.5 times larger than the test case of 50 µm, albeit with the parameters of that section.

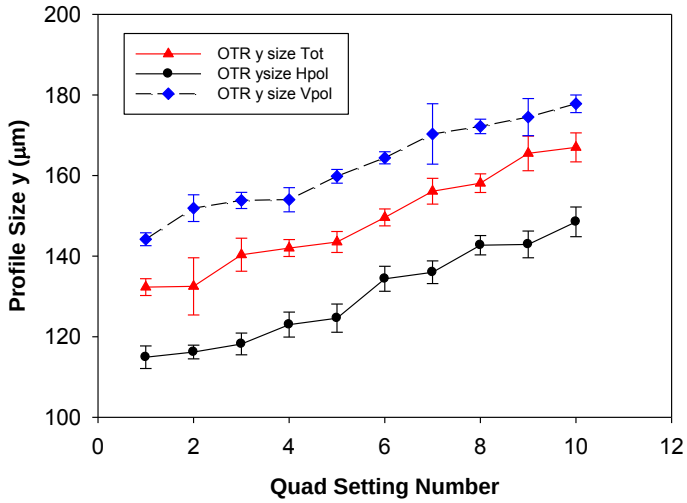

Figure 9: Comparison of the total OTR projected profiles in y (red), horizontally polarized (Hpol) results (black), and vertically polarized (Vpol) OTR results (blue) as a function of upstream quadrupole (Quad) settings at 4.5 GeV.

7-GeV CASE (APS/ANL)

Several years ago, a first series of experiments was done on the demonstration of near-field imaging of 7-GeV beams at APS with ODR-based techniques [15]. Fundamental to these studies was the imaging of linearly polarized ODR components and referencing to the OTR image sizes at the same diagnostics station. In the course of these tests, we also recorded polarized images of OTR as tabulated in Table 4. Even though the horizontal size was over 1100 µm, we still noticed clear image-size reductions of 15% with the perpendicularly polarized component as shown in Fig. 10 and as now reported for the first time. The projected horizontal profiles of the 10-image sums show the total OTR (black curve) result with the vertically polarized profile (red curve) width being detectably smaller! The profile intensities and baseline were scaled and shifted, respectively, to make the direct comparison. The effect persisted in the smaller vertical dimension at 251 µm as well with a ~16% reduction to 212 µm. We have revisited the 10-image sets to establish the statistical uncertainty in the measurements which are included in Table 4.

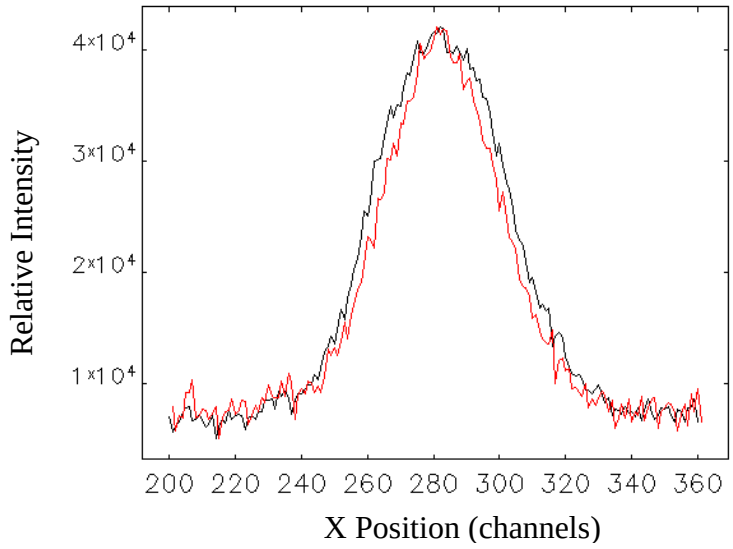

Figure 10: Comparison of the projected OTR x profiles using no polarizer (black) and the vertical polarizer (red). The perpendicular component's width is ~15% smaller than the total OTR case. The beam sizes are from the 10-image sum as given in Table 4.

Table 4: Summary of 7-GeV APS OTR data with 3.2 nC. The horizontal (H) polarization data are indicated in determining the y sizes and vice versa with the vertical (V) polarization data. The first three data rows are based on 10-image sums, and then the 10 images were processed individually to determine the averages and the statistical errors.

Polarization	**X-sigma (pixel)**	**X-sigma (μm)**	**Y-sigma (pixel)**	**Y-sigma (μm)**
No	19.6	1176	5.4	**248**
H	18.1	1086	4.5	**207**
V	16.6	996	5.4	**248**
Averages				
No	19.2 ±0.24	1152±14	5.46±0.10	251±5
H	18.3 ±0.29	1101±17	4.60±0.06	212±3
V	16.7 ±0.15	1004±10	5.42±0.13	250±5

V. DISCUSSION

If one then collects examples from the three experiments at FNAL, JLAB, and APS, the empirical evidence indicates basically a gamma-independent effect as seen in Table 5 where similar fractional effects were observed at 14 MeV and 4.5 GeV in the 125-μm size regime [21,16]. In these PSF case calculations we used the θ_{max}= 20 mrad, the same as the JLAB experiment and our estimates for the other two experiments with a final lens with aperture. Experimentally, we can only obtain the total OTR image and the linearly polarized components of it so we reference the fractional size reduction to change to the total OTR image size in column 2. Moreover, the profile differences scale with the beam image size so the fractional reduction is very similar at ~13-18% in the experimental results of Columns 2-4. Only when the PSF width is close to the actual beam size from the polarized PSF or single particle function of references [5] and [6], respectively do we calculate larger effects. We see the

growth of the PSF effects at 25 and 10 μm with θ_{max}= 10 mrad as in Section III. The magnitude of the difference is 4-5 times the modeled result in general. It is consistent with the induced current distributions being larger than the actual charge distribution. Also, the perpendicular PSF has not been deconvolved yet, so the actual beam size is even smaller presumably as indicated by the results shown in Columns 4-8. In principle, the PSF could be determined quantitatively by using a delta-function-like beam size in the few-μm regime to visualize it as done by Aryshev et al.[19]. In practice, we generally cannot generate such small beams in many of our accelerators, or if we do, the charge is then too low to image readily.

Table 5. Summary of results from the three series of experiments ordered by increasing total OTR image sigma size. The fractional reductions obtained with the perpendicular component compared to the total OTR are 5-10 times larger in these experimental cases in Column 4 than in the calculated OTR PSF convolution cases in Column 8.

	Experimental Results			**OTR PSF Model Convolution Results**			
Beam energy (GeV)	**Total OTR Sigma (μm)**	**Perpendicular OTR Sigma: x,y (μm)**	**Fractional Size Reduction (%)**	**Initial Sigma (μm)**	**Total OTR Sigma Calc. (μm)**	**Perpendicular OTR Sigma Calc. (μm)**	**Calc. Size Reduction (%)**
0.014	67	55	18	50	52	51	2
0.014	125[a]	101[a]	19	100	102	101	1
4.5	149	124	17	125	138	133	3
4.5	157	130	17	125	138	133	3
7.0	251	212	16	200	216	209	3
7.0	1150	1004	13	1000	1027	1014	1

a) Ref.17

For those investigators familiar with the near-field optical diffraction radiation (ODR) experiments at high gamma at APS and JLAB, we had observed a similar pattern where the perpendicular component

always resulted in a narrower ODR image in the x plane. The linear polarizers were installed for the ODR tests with OTR images to be used as a reference. One existing model for ODR is reported in [15], and it clearly shows significant differences between the parallel and perpendicular polarization components computationally for the transverse profiles and as observed experimentally [15,16]. Since a single plane screen whose edge was positioned above the beam by ~1 mm was used, and thus broke vertical symmetry, the vertically polarized component was a single lobe and the parallel polarization was a weaker-in-intensity double lobe as shown in Fig. 11. This simulation is at 7 GeV for a 20-µm sigma initial beam size in x and y and the 100-µm impact parameter [20]. We routinely used the vertically polarized ODR images that were smaller in the x–dimension than the total ODR image for monitoring x-beam size. We also acquired the reference OTR images without and with polarizers inserted. (Note: Although qualitatively in the correct sense, the slight reduction in image size in an optical system by only a few wavelengths in magnitude with use of the linearly polarized light perpendicular to a dimension of interest as described in M. Mansuripur's book [21] is discounted for explaining the much larger experimental effects observed in this study.)

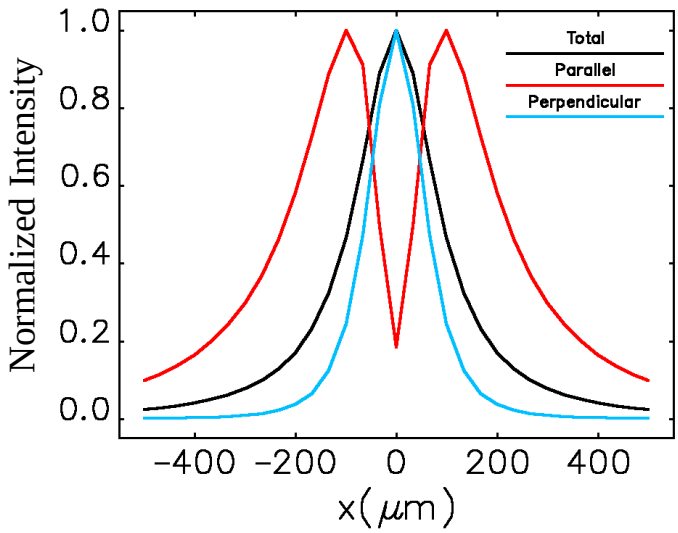

Figure 11: Comparison of different ODR polarization components with normalized intensities: Total (black), perpendicular (blue), and parallel (red). The actual Gaussian beam size is 20 µm, the height is 20 µm, and the impact parameter is 100 µm. [20].

VI. SUMMARY

In summary, we have detected an apparent polarization-dependent beam profile size for OTR images of relativistic electron beams. At low energy we see projected profile reductions of 18% in x and 10% in y relative to the total radiation image profile at 14.3 MeV. The observed asymmetry of the effect at γ~30 is not readily addressed in the PSF model with the OTR screen at an angle. Similar polarization effects were observed over a wide range of gamma from ~30-14,000 and beam sizes from ~50 to 1200 µm. The magnitude of the experimental effect is only approached in the PSF model by reducing the solid angle subtended by the optics and reducing the beam size, but still a simple convolution would not explain the systematic fractional effect magnitudes at beam sizes >100 µm, much less at 1200 µm. We find that the OTR polarization effects are qualitatively analogous to what was observed in ODR near-field experiments in the past [15] which may be attributed to the time-dependent induced-current distribution in the metal surface which we time average in the CCD camera. We recommend the use of the OTR perpendicular component relative to the beam dimension at a minimum and the subsequent deconvolution of that component's contribution when known. We will continue investigations with the imaging stations on the Advanced Superconducting Test Accelerator (ASTA) now under construction with expected beam energies of 50 to 800 MeV, and we encourage other investigators to assess such effects in their experiments including that of high dynamic range beam-halo imaging with OTR.

VII. ACKNOWLEDGEMENTS

The authors acknowledge support from N. Eddy and M. Church and the technical assistance of J. Santucci of Fermilab. The first author also acknowledges various discussions on OTR with H. Loos and J. Frisch,of SLAC, with R. Fiorito of the Univ. of Maryland, and with D. Rule of NSWC.

VIII. REFERENCES

[1] L. Wartski et al., Journ. Appl. Phys., **46**, 3644 (1975).

[2] R.B. Fiorito and D.W. Rule, p.21, Conf. Proc. No.319, BIW94, Robert E. Shafer, ed. AIP (1994).

[3] A. H. Lumpkin et al., "Initial Imaging of 7-GeV Electron Beams with OTR/ODR Techniques at the APS", Proc. of PAC05, Knoxville, Tenn., p.4162. (2005), http://www.JACoW.org.

[4] V.A. Lebedev, Nucl. Instr. in Phys. Res. **A372**, 344 (1996).

[5] X. Artru, R.Chehab, K.Honkavarra, and A.Variola, Nucl. Instr. and Methods,B145, 160 (1998).

[6] M. Castellano and V.A.Verzilov, Phys. Rev. ST Accel. Beams, 1:062801 (1998).

[7] Dao Xiang,. Wen-Hui Huang, and Yu-Zheng Lin, Phys. Rev. ST Accel. Beams **10,** 062801 (2007).

[8] M. Borland et al., Proc. 2001 PAC, 2707-2709 (2001); M. Borland et al., Nucl. Instr. Methods Phys. Res. Sect. A **483**, 268 (2002).

[9] E.L. Saldin, E.A. Schneidmiller, and M.V. Yurkov, Nucl. Instr. Methods Phys. Res. Sect. A **490**, 1 (2002).

[10] Z. Huang et al., Phys. Rev. ST-AB **7**, 074401 (2004).

[11] R. Akre et al., Phys.Rev.ST-AB **11**, 030703 (2008).

[12] A.H. Lumpkin, R.J. Dejus, and N.S. Sereno, "COTR and SASE Generated by Compressed Electron Beams", Proc. of FEL08, Kyeongju, Korea, August 26-30, 2008. http://www.JACoW.org.; A.H. Lumpkin, R.J. Dejus, and N.S. Sereno., Phys. Rev. ST-AB **12**, 040704 (2009).

[13] A.H. Lumpkin et al., "OTR Polarization effects in Beam profile Monitors at the Fermilab A0 Photo-injector", Proc. of BIW10, May 2010, Santa Fe, NM, TUPSM001, http://www.JACoW.org.

[14] A.H. Lumpkin et al., "Initial Beam-Profiling Tests with the NML Prototype Station at the Fermilab A0 Photoinjector" , Proc. of PAC11, New York, NY, MOP219, (2011), http://www.JACoW.org.

[15] A.H. Lumpkin at al., Phys. Rev. ST-AB, **10**, 022802, (2007).

[16] P. Evtushenko, A.H. Lumpkin, A.P. Freyberger, and C. Y. Liu, "Near-Field ODR Measurements at CEBAF", Proc. of BIW08, Lake Tahoe, CA, WECOTC01, p.332, (2008), http://www.JACoW.org

[17] A.H. Lumpkin et al., Phys. Rev. ST-AB 14, 060704 (2011).

[18] Alex H. Lumpkin, Proc. of BIW12, Newport News, VA, TUBP02, (2012) http://www.JACoW.org

[19] A. Aryshev et al., Proc. of IPAC10, Kyoto, Japan, MOPEA052, 195 (2010), http://www.JACoW.org.

[20] C.-Y. Yao, A.H. Lumpkin, and D.W. Rule, Proc of PAC07, Albuquerque NM, FRPMS001 (2007), http://www.JACoW.org.

[21] Masud Mansuripur, *Classical Optics and its Applications*, Cambridge Press 2009, Chapter 3.